The Cerebellum (2019) 18:372–387
https://doi.org/10.1007/s12311-018-1003-9

ORIGINAL PAPER

Age-Dependent White Matter Characteristics of the Cerebellar Peduncles from Infancy Through Adolescence

Lisa Bruckert[1] · Katie Shpanskaya[2] · Emily S. McKenna[2] · Lauren R. Borchers[1] · Maya Yablonski[3] · Tal Blecher[3] · Michal Ben-Shachar[3,4] · Katherine E. Travis[1] · Heidi M. Feldman[1] · Kristen W. Yeom[2]

Published online: 14 January 2019

Abstract

Cerebellum-cerebrum connections are essential for many motor and cognitive functions and cerebellar disorders are prevalent in childhood. The middle (MCP), inferior (ICP), and superior cerebellar peduncles (SCP) are the major white matter pathways that permit communication between the cerebellum and the cerebrum. Knowledge about the microstructural properties of these cerebellar peduncles across childhood is limited. Here, we report on a diffusion magnetic resonance imaging tractography study to describe age-dependent characteristics of the cerebellar peduncles in a cross-sectional sample of infants, children, and adolescents from newborn to 17 years of age ($N = 113$). Scans were collected as part of clinical care; participants were restricted to those whose scans showed no abnormal findings and whose history and exam had no risk factors for cerebellar abnormalities. A novel automated tractography protocol was applied. Results showed that mean tract-FA increased, while mean tract-MD decreased from infancy to adolescence in all peduncles. Rapid changes were observed in both diffusion measures in the first 24 months of life, followed by gradual change at older ages. The shape of the tract profiles was similar across ages for all peduncles. These data are the first to characterize the variability of diffusion properties both across and within cerebellar white matter pathways that occur from birth through later adolescence. The data represent a rich normative data set against which white matter alterations seen in children with posterior fossa conditions can be compared. Ultimately, the data will facilitate the identification of sensitive biomarkers of cerebellar abnormalities.

Keywords Cerebellum · Development · Diffusion MRI · Tractography · White matter · Children and adolescents

Introduction

The cerebellum is a division of the human brain, situated below the cerebral hemispheres in the posterior fossa. Its distinctive anatomical structure is comprised of a continuous, tightly folded cortical sheet that contains over 50% of the neurons in the human brain, while accounting for only 10% of the brain's volume. The cerebellum plays an important role in motor control and motor-learning, cognition, and emotion [1–4]. Damage to the cerebellum can lead to deficits in higher cognitive functions and emotional expression, a condition described as the cerebellar cognitive affective syndrome [5–7]. Study of the cerebellum in children is highly important because many disease processes injure the cerebellum during childhood [6, 8]. Pediatric brain tumors commonly affect the cerebellum [9]. Abnormal cerebellar development is a complication of extreme prematurity [10–12] and has been associated with poor developmental outcomes [11]. In addition,

Electronic supplementary material The online version of this article (https://doi.org/10.1007/s12311-018-1003-9) contains supplementary material, which is available to authorized users.

✉ Heidi M. Feldman
hfeldman@stanford.edu

[1] Division of Developmental-Behavioral Pediatrics, Stanford University School of Medicine, Stanford, CA 94305, USA

[2] Department of Radiology, Lucile Packard Children's Hospital, Stanford University School of Medicine, Stanford, CA 94305, USA

[3] The Gonda Multidisciplinary Brain Research Center, Bar Ilan University, 5290002 Ramat Gan, Israel

[4] Department of English Literature and Linguistics, Bar Ilan University, 5290002 Ramat Gan, Israel

cerebellar injury or dysmaturity has been implicated in developmental disorders, such as autism [13].

The cerebellum is linked to the cerebrum and to the spinal cord by numerous axons that are grouped together in three major white matter bundles: the middle (MCP), inferior (ICP), and superior cerebellar peduncles (SCP) [14]. The MCP is a major afferent pathway in which input fibers run from the contralateral cerebral cortex via pontine nuclei across the midline of the cerebellum to the cerebellar cortex [14]. The left and right ICP are major afferent pathways, feeding signals from the spine and the olivary nucleus into the cerebellum, and efferent pathways from the cerebellum towards the vestibular nuclei along the border of the pons and medulla [14]. The left and right SCP are primarily efferent pathways that emerge from the deep cerebellar nuclei, travel into the dorsal pons, decussate at the level of the inferior colliculus, and continue via the thalamus to the contralateral cerebral cortex [14]. These pathways can be interrogated using diffusion magnetic resonance imaging (dMRI)—the leading tool used to investigate white matter properties non-invasively, in vivo. Tractography allows identification and characterization of specific white matter pathways, including the cerebellar peduncles [15].

Studies of the cerebellar structure in children and adolescents have considered the size or volume of the entire cerebellum [16, 17], selected anatomical compartments [18], lobular structures [19], and myelin water fraction [20]. DMRI metrics such as fractional anisotropy (FA) and mean diffusivity (MD) provide sensitive markers of white matter changes across ages that cannot be detected on conventional MRI [21, 22]. Saksena and colleagues [23] applied a region of interest approach to dMRI data in children from 6 days to 11 years to compare age-related differences in FA and MD of cerebral and cerebellar white matter. They found rapid initial change and then slow development after age 3 years. Two studies in older children and adolescents applied a reliable and reproducible method for reconstructing and quantifying diffusion properties along the trajectory of white matter pathways to generate tract profiles of the cerebellar peduncles [24, 25]. The studies found no age-dependent differences in FA of any of the peduncles in these 9–17-year-old children.

The first goal of the present study was to apply dMRI tractography to the cerebellar peduncles to assess age-related differences in mean tract-diffusion properties (FA, MD) across the entirety of childhood, from infancy through adolescence. Based on previous findings, we predicted that (i) mean tract-FA would increase from infancy to adolescence, (ii) mean tract-MD would decrease from infancy to adolescence, and (iii) that the logarithmic fit would describe these age-related differences in diffusion properties. The second goal was to examine the variability in FA/MD within five different age groups. We tested whether these age groups showed significant differences in mean tract-FA/MD values. Further, we wanted to explore whether these diffusion properties would vary similarly along the trajectory of each cerebellar peduncle among the age groups, creating similar tract profiles across ages. Based on increasing FA in older as compared to younger children in cerebral tracts [26], we hypothesized similar trajectories for the cerebellar peduncles.

The significance of this study is to provide a normative dataset of the growth of the cerebellar peduncles from infancy through adolescence. Describing age-related differences in these pathways is likely to inform understanding for how the cerebellum contributes to the development of specific motor and cognitive behaviors in children. Quantifying age-related differences in white matter microstructure in typically developing children is also a necessary prerequisite to understanding variations in cerebellar white matter development in clinical populations. Deviations from the normal pattern of white matter development may lead to reduced brain connectivity. Aberrant development may also result in dis-synchronous communication between gray matter regions, which is thought to result in abnormal motor, cognitive functioning, and behaviors observed in a variety of neurological and psychiatric disorders [27, 28]. Comparing diffusion metrics in abnormal clinical populations to typically developing children may lead to identification of biomarkers for specific conditions.

Methods

Participants

Medical records and dMRI scans from children and adolescents who presented at the Lucile Packard Children's Hospital at Stanford for brain MRI between January 2010 and November 2017 were retrospectively reviewed after institutional review board (protocol 28674) approval. MRI studies conducted between December 2013 and July 2016 had to be excluded due to infrastructural scanner challenges that prohibited the acquisition of advanced diffusion imaging. Despite this interruption, there was no change in scanner hardware during the study period. At our institution, high-resolution structural and diffusion imaging is part of the routine pediatric brain MRI protocol for a variety of clinical indications. Because clinical data might be inconsistent or incomplete, and because individuals who underwent clinical MRI might be at risk for abnormalities, we performed three rounds of reviews to select the final study cohort (Fig. 1). First, we identified 1142 individuals aged between 1 day and 17 years of age who had obtained both high-resolution T1-weighted volumetric and diffusion MRI imaging at 3 T. Second, a board-certified pediatric neuroradiologist (K.W.Y. with > 8 years of dedicated experience) reviewed all MRI scans. Scans that showed specific brain abnormalities, such as tumor, hemorrhage, stroke, brain malformations,

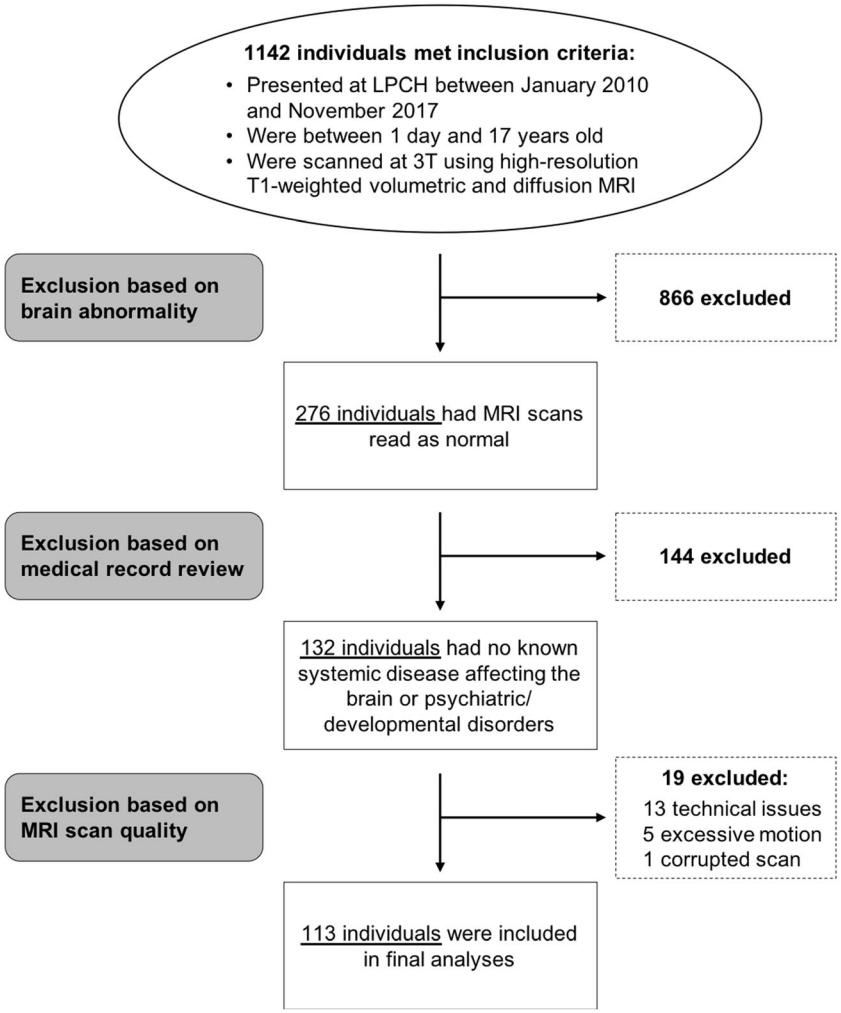

Fig. 1 Flow chart describing inclusion and exclusion criteria of participants in this study. LPCH = Lucile Packard Children's Hospital Stanford

hydrocephalus, prior injury, nonspecific focal white matter signal abnormality, or other nonspecific or benign imaging features, such as arachnoid cyst, were excluded ($n = 866$). Third, we performed a thorough clinical chart review to ensure that individuals were included only if the initial assessment and follow-up reports did not lead to a clinical diagnosis that might affect the cerebellum. We excluded individuals with a history of prematurity, hearing loss, abnormal developmental (motor or language), emotional, or behavioral conditions (e.g., autism, attention deficit/hyperactivity disorder), genetic, endocrine, neurological, or psychiatric disorders, chronic medical therapy, or other systemic diseases affecting the brain ($n = 144$). Clinical indications for MRI assessments in the remaining 132 individuals included isolated headaches, nausea, scalp nevus, peri-orbital dermatoid, facial hemangioma, benign strabismus without orbital or intracranial abnormality, sinus disease or inflammatory nasal obstruction, ear infection, syncope without a history of generalized seizures, and family history of aneurysm or vascular malformations. We excluded diffusion scans that were affected by technical issues during acquisition ($n = 13$), corrupted ($n = 1$), or affected by excessive motion ($n = 5$). Our final sample included 113 individuals aged 1 day to 17 years ($M_{age} = 7, 3$; $SD_{age} = 6, 6$; 55 males). Inter-rater reliability on > 25% of the medical records ($n = 30$) yielded 93.3% agreement. Therefore, we accepted the first reviewer's decision and all 113 cases remained in the data set. Because all included brain scans were read as normal and follow-up medical assessments did not lead to a clinical diagnosis, no individual was scanned twice. The age distributions can be seen in Fig. 2.

MRI Data Acquisition

All MRI scans were obtained at 3 T (GE MR750 Discovery; GE Healthcare, Waukesha, WI, USA) using an 8-channel head coil. Children younger than 3 months of age were scanned using a swaddle-and-feed method; children aged 3 months to 6 years of age were sedated under general anesthesia; and some children aged 6–8 years were sedated based on individual maturity level and ability to tolerate the MRI exam. It is highly unlikely that anesthesia affected these structural scans because of the brief time lag between medication

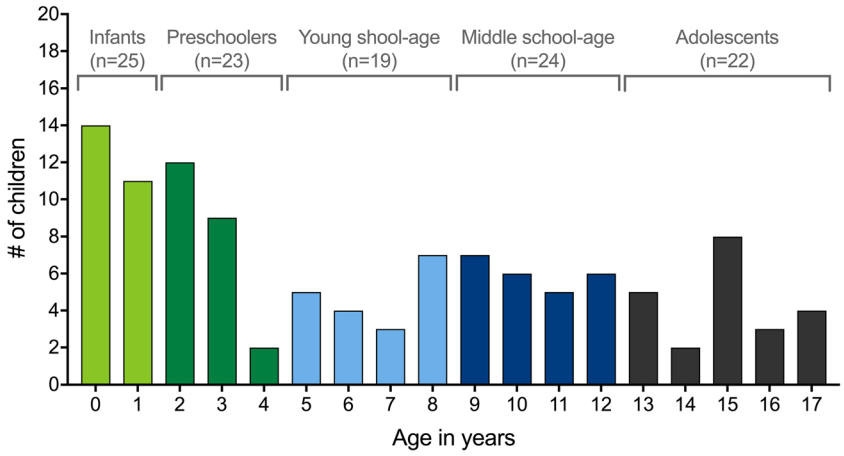

Fig. 2 Age distribution and age groupings of all included individuals ($n = 113$)

administration and scan acquisition. Both high-resolution T1-weighted (3D SPGR, TR = 7.76 ms, TE = 3.47 ms, FOV = 240 × 240 mm^2, acquisition matrix = 512 × 512, voxel size = 0.4688 × 0.4688 × 1 mm^3, orientation = axial) and diffusion-weighted images were acquired as part of the pediatric brain MRI protocol. Diffusion data were collected with a twice-refocused GRAPPA DT-EPI sequence (TR = 4000–6000 ms depending on slice coverage, TE = 76.59 ms, FOV = 240 × 240 mm^2, acquisition matrix = 256 × 256, voxel size = 0.9375 × 0.9375 × 3 mm^3) using a b-value of 1000 s/mm^2 sampling along 25 isotropically distributed diffusion directions. One additional volume was acquired at b = 0 at the beginning of each scan.

MRI Data Preprocessing

DMRI data were pre-processed using the open-source software mrDiffusion (http://github.com/vistalab/vistasoft/mrDiffusion) implemented in MATLAB R2014a (MathWorks, Natick, MA, USA). To correct for participants' motion, we applied a rigid body transformation [29] to register each diffusion-weighted image to the non-diffusion (b0) image. The b0 image was registered to the participant's T1-weighted image, which had been aligned to the canonical AC-PC orientation. The combined transform that resulted from motion correction and alignment to the T1-weighted image was applied to the raw data once, and the transformed images were resampled to 2 × 2 × 2 mm isotropic voxels. This step was performed because non-isotropic voxels may bias the tensor fitting algorithm and distort both tracking and measurements of diffusion properties [30]. Diffusion gradient directions were then adjusted to fit the resampled diffusion data [31]. Maps of FA and MD were generated using a standard least squares algorithm.

All dMRI scans were rigorously assessed for relative head motion. We quantified the degree of relative head motion in each participant by calculating the magnitude of motion correction (in voxels) in the x-y-z plane of each volume relative to the prior volume. For each dMRI scan, we counted the number of volumes with translational motion of 1 voxel or more, relative to the prior volume. We then calculated the mean number of volumes with ≥ 1 voxel of relative motion across the entire sample ($M = 1.48$, $SD = 3.00$). Participants who deviated from this mean by more than three standard deviations were excluded from analyses (five participants). Group comparisons were also performed to ensure that infants, preschoolers, young school-aged children, middle school-aged children, and adolescents did not differ in their relative head motion.

White Matter Tract Identification

The open-source software, Automated Fiber Quantification (AFQ), was used to track and segment cerebellar white matter pathways in each participant's native space. The methods and algorithms used in AFQ have been described in detail by [26]. In brief, AFQ consists of three main processing steps: (i) whole-brain tractography, (ii) automatic tract segmentation using template regions of interest (ROIs) warped to native space, and (iii) automatic tract refinement and cleaning [26]. For the deterministic streamline tracking algorithm [32], the default tracking parameters were adjusted based on FA values utilized in previous dMRI studies of neonates in order to balance the inclusion of less mature white matter regions in very young infants while minimizing the inclusion of gray matter and partial volume effects [33, 34]. The tracking algorithm was seeded with a white matter mask defined as all the voxels with FA value greater than 0.15. Tracking proceeded in all directions and stopped when FA dropped below 0.10 or when the angle between the last path segment and next step direction was greater than 30°. Fiber tract segmentation was based on waypoint ROIs, which were defined on the JHU MNI template following the procedure described by Travis et al. [25]. ROI placement in the template was verified by a clinical pediatric neuroradiologist.

We implemented a novel and automated method for segmentation of the cerebellar peduncles in AFQ. Using this

method, the left and right ICP were segmented by drawing one ROI on the ICP on an axial plane at the level of the medulla (inferior to the dentate nucleus) and the second ROI on the ipsilateral ICP on an axial plane at the level of the ponto-mesencephalic junction. The left and right SCP were segmented by drawing one ROI on the dentate nucleus on an axial plane at the level of the medial pons and another ROI on the ipsilateral SCP on an axial plane at the level of the ponto-mesencephalic junction. The MCP was segmented by drawing two ROIs within the cerebellum on an axial plane at the level of the medial pons: one placed on the central portion of the right MCP and the other placed on the central portion of the left MCP. A non-linear transformation [35] was applied to warp these ROIs from the MNI template space into each individual's native space. In the waypoint ROI procedure, each fiber from the whole-brain tractogram becomes a candidate for a specific fiber group if it passes through two ROIs that define the trajectory of the fiber group. The core of the tract was calculated by defining 30 sample points along the tract and computing the robust mean position of the corresponding sample points. The robust mean was computed by estimating the three-dimensional Gaussian covariance of the sample points and removing fibers that were either more than 4 standard deviations away from the mean position of the tract or that differed more than 1 standard deviation in length from the mean length of the tract for relatively short cerebellar pathways. This method was successfully used for cerebral tract segmentation in younger children and toddlers [36, 37]. Further, we carried out a validity check of the cerebellar tract segmentation in an independent sample of 42 children and adolescents aged 9–16 years [25]. We compared mean tract-FA and mean tract-MD derived from our automatically segmented MCP, left/right ICP, and left/right SCP to those derived from manually segmented peduncles. We found that both diffusion metrics were highly correlated across subjects using the two methods (FA: $0.80 < r < 0.98$, $p < 0.0001$; MD: $0.88 < r < 98$, $p < 0.0001$). Fiber renderings for each tract and each child were visually inspected prior to any statistical analyses to ensure that each tract conformed to anatomical norms. Using these methods, we were able to identify the cerebellar peduncles in the majority of children. A small number of children were excluded from each analysis because a tract could not be segmented or did not conform to anatomical norms: excluded were three (all infants) from the MCP, six (three infants, two preschoolers, and one young school age) from the left ICP, seven (five infants and two preschoolers) from the right ICP, two (one infant and one preschooler) from the left SCP, and three (two infants and one preschooler) from the right SCP. Only one child was excluded from multiple tracts. Diffusion properties (FA, MD) were quantified at 30 equidistant nodes along the central portion of each fiber tract bounded by the same two ROIs used for tract segmentation (Fig. 3). Mean tract-diffusion indices were calculated by averaging FA or MD values of all 30 nodes.

Statistical Analyses

Statistical analyses were conducted using IBM SPSS software (version 23.0, IBM Corporation, 2014). Statistical significance was set at $p < 0.05$. The Shapiro-Wilk test was used to assess whether mean tract-diffusion indices were normally distributed. Independent *t* tests were used to examine whether mean tract-diffusion measures of the MCP, ICP, and SCP differed between male and female participants across the entire sample. Based on previous findings by Saksena et al. [23] and Deoni et al. [20], logarithmic curve estimations were used to explain the relation between age (in months) and mean tract-diffusion indices (FA, MD):

$$y = b_0 + (b_1 \times \ln(x))$$

In this equation, y is the estimated DTI value, x is the age, b_0 is the constant term, and b_1 is the regression coefficient of the log transform of age. For each model regression coefficients, R^2 and 95% confidence interval of the means were estimated.

To describe age-related differences, we divided the sample into five age groups (years, months) of comparable size (Fig. 2): infants (0, 0–1, 11; $M_{age} = 1; 0$; 14 males), preschoolers (2, 0–4, 11; $M_{age} = 3, 3$; 14 males), young school age (5, 0–8, 11; $M_{age} = 7, 0$; 5 males), middle school age (9, 0–12, 11; $M_{age} = 10, 10$; 10 males), and adolescents (13, 0–17, 11; $M_{age} = 15, 4$; 12 males). Analyses of variance (ANOVA) were conducted to examine the effect of sex and age group on mean tract-FA and MD separately for the MCP, ICP, and SCP. Levene's test was used to examine homogeneity of variances. If the assumption of homogeneity of variance was not violated, we used Tukey for post hoc comparisons. If the assumption of homogeneity of variances was violated, we interpreted the results of the Welch ANOVA and used Games-Howell for post hoc comparisons.

Results

Mean Tract-FA and MD Values Across the Sample

No significant differences in mean tract-FA or mean tract-MD of the MCP, left/right ICP, and left/right SCP were found between male and female participants (Online Resource 1). We therefore examined mean tract-diffusion values across sexes.

Mean tract-FA across all ages was highest in the MCP, followed by the ICP and SCP (Table 1). When plotting mean tract-FA of the cerebellar peduncles against age for all participants, we detected an initial sharp increase in FA over the first

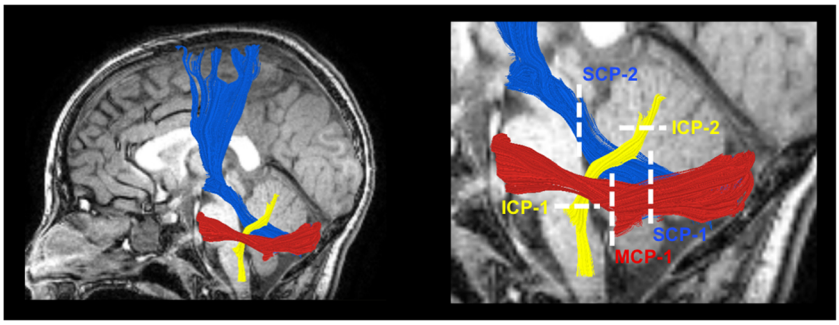

Fig. 3 Tractography of the cerebellar peduncles. Tract renderings of the middle (MCP, red), inferior (ICP, yellow), and superior (SCP, blue) cerebellar peduncles are shown on a T1-weighted image of a representative subject (40 months old). Only tract renderings for the left hemisphere are shown (sagittal view). White dashed lines indicate the location of the two ROIs used to identify each cerebellar peduncle

24 months, followed by a gradual increase in later ages. Figure 4 shows that mean tract-FA ranged from 0.17 to 0.28 at birth and reached a relative plateau at around 0.50 for the MCP and 0.40 for the ICP and SCP after 70 months of age. As hypothesized, logarithmic models provided a significant fit and explained approximately 42%, 39%, 46%, 49%, and 50% of the variance in mean tract-FA of the MCP, left ICP, right ICP, left SCP, and right SCP, respectively (Table 1).

Mean tract-MD across all ages was highest in the SCP, followed by the MCP and then ICP (Table 2). Figure 5 shows that tract-MD of the cerebellar peduncles decreased sharply over the first 24 months. This decrease stabilized after 70 months of age at around 0.90 for the MCP, 0.80 for the ICP, and 1.05 for the SCP. As with tract-FA, logarithmic models provided a significant fit and explained approximately 25%, 32%, 47%, 23%, and 15% of the variance in mean tract-MD of the MCP, left ICP, right ICP, left SCP, and right SCP respectively (Table 2).

Age-Related Differences in Cerebellar Tract Profiles

In preliminary analyses, we found that the average relative head motion was minimal in all age groups ($M \pm SD$: infants 0.26 ± 0.17 voxels, preschoolers 0.26 ± 0.16 voxels, young school age 0.25 ± 0.12 voxels, middle school age 0.19 ± 0.11 voxels, adolescents 0.16 ± 0.10 voxels) and that it did not significantly differ among groups ($p > 0.05$). FA values of the cerebellar peduncles were normally distributed within each age group for the MCP, right ICP, and right SCP, with the only exceptions being left ICP in infants and left SCP in middle school age. MD values of the cerebellar peduncles were also normally distributed within each age group for the MCP and right SCP, with the exceptions being the left ICP (preschoolers, middle school age), right ICP (preschoolers), or right SCP (infants). Therefore, we used parametric statistics for analyses but confirmed statistical significance with non-parametric statistics. The assumption of homogeneity of variances was violated for tract-FA values of the left SCP and MCP as well as tract-MD values of the left and right ICP and MCP (Table S1). We varied the post hoc analyses accordingly.

There was no main effect of sex (FA: $0.329 < p < 0.600$; MD: $0.391 < p < 0.951$) and no significant interaction between sex and age group (FA: $0.648 < p < 0.920$; MD: $0.525 < p < 0.852$) on mean tract-FA or MD of the MCP, left and right ICP, and left and right SCP.

Mean tract-FA differed significantly among the five age groups (Online Resource 2). As expected, tract-FA increased from infancy to adolescence across all peduncles (Table 3). In the MCP, we observed a significant increase in tract-FA from infants to preschoolers and from preschoolers to young school-aged children, but an apparent decrease was observed

Table 1 Mean tract-FA of cerebellar pathways across all ages and summary of logarithmic curve model fit of age in relation to mean tract-FA

	Tract-FA ($M \pm$ SD)	Model summary			Parameter estimates	
		R^2	F	p value	b_0	b_1
MCP	0.48 ± 0.07	0.417	77.2	0.000	0.307	0.041
ICP-L	0.39 ± 0.07	0.389	66.8	0.000	0.266	0.031
ICP-R	0.40 ± 0.07	0.465	90.4	0.000	0.260	0.034
SCP-L	0.39 ± 0.07	0.493	106.1	0.000	0.255	0.034
SCP-R	0.38 ± 0.06	0.504	109.5	0.000	0.255	0.032

FA fractional anisotropy, *MCP* middle cerebellar peduncle, *ICP* inferior cerebellar peduncle, *SCP* superior cerebellar peduncle, *L* left, *R* right

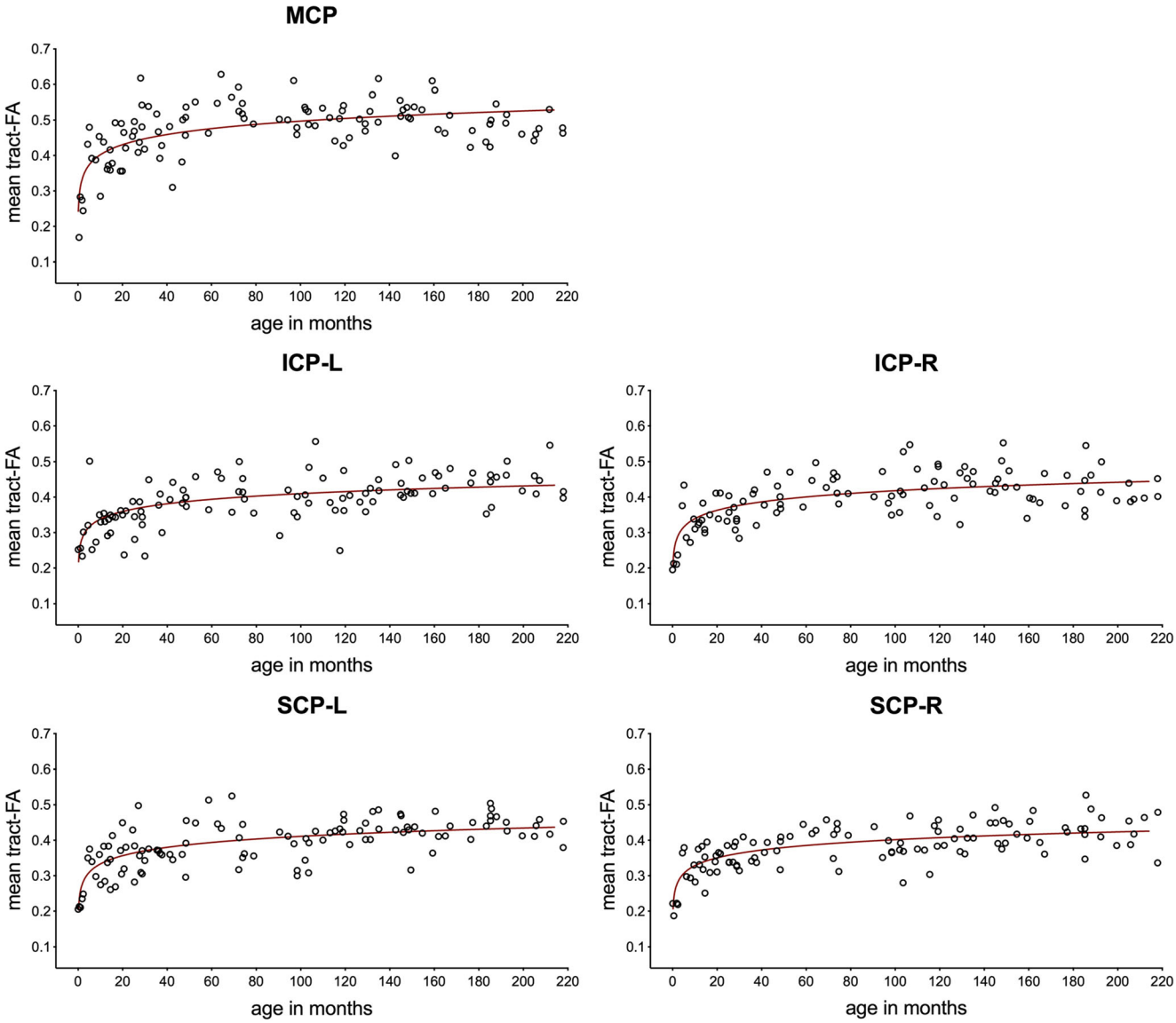

Fig. 4 Relationship between mean tract fractional anisotropy (FA) and age in the cerebellar peduncles of children ranging in age from birth to 17 years (214 months). Red line shows the logarithmic curve estimation. *MCP* middle cerebellar peduncle, *ICP* inferior cerebellar peduncle, *SCP* superior cerebellar peduncle, *L* left, *R* right

from young school-aged children to middle school-aged children and adolescents. The decrease in tract-FA did not reach statistical significance (Fig. 6). In the left and right ICP, tract-FA also increased from infants to preschoolers and from preschoolers to young school-aged children or adolescents. Tract-FA did not significantly differ between school-aged children and adolescents (Fig. 6). In the left and right SCP, there was a significant increase in tract-FA from infants to preschoolers but not from preschoolers to young school-aged children. Interestingly, tract-FA increased from preschoolers and young school-aged children to middle school-aged children and adolescents (Fig. 6).

Mean tract-MD of each cerebellar peduncle also differed significantly among the five age groups (Online Resource 2). From infancy to adolescence, tract-MD decreased across all peduncles (Table 4). In the MCP, we saw a significant decrease in tract-MD from infants to preschoolers and from preschoolers to school-aged children. From school-aged children to adolescents, tract-MD marginally increased again (Fig. 7). In the left and right ICP, tract-MD did not significantly differ between infant and preschoolers. However, there was a significant decrease in tract-MD from infants/preschoolers to young school-aged children, middle school-aged children, and adolescents (Fig. 7). In the left and right SCP, we observed a

Table 2 Mean tract-MD of cerebellar pathways across all ages and summary of logarithmic curve model fit of age in relation to mean tract-MD

	Tract-MD ($M \pm$ SD)	Model summary			Parameter estimates	
		R^2	F	p value	b_0	b_1
MCP	0.93 ± 0.15	0.253	36.3	0.000	0.999	− 0.001
ICP-L	0.84 ± 0.10	0.323	50.1	0.000	1.004	− 0.042
ICP-R	0.81 ± 0.10	0.475	94.0	0.000	1.002	− 0.048
SCP-L	1.04 ± 0.12	0.233	33.1	0.000	1.201	− 0.040
SCP-R	1.07 ± 0.12	0.154	19.6	0.000	1.209	− 0.034

MD mean diffusivity, *MCP* middle cerebellar peduncle, *ICP* inferior cerebellar peduncle, *SCP* superior cerebellar peduncle, *L* left, *R* right

similar pattern: infants and preschooler did not significantly differ in tract-MD, but tract-MD decreased from infants/preschoolers to middle school-aged children and adolescents. There were no significant differences between school-aged children and adolescents (Fig. 7).

Because some diffusion measures were not normally distributed, we repeated the analyses using the Kruskal-Wallis test. For all cerebellar peduncles, the test replicated significant differences in tract-FA and tract-MD between the age groups (Online Resource 3). The pattern of post hoc comparisons, as assessed by Dunn's procedure with a Bonferroni correction, did not change (Online Resources 4 and 5).

Visual inspection of the tract profiles (Figs. 6 and 7) revealed that the overall shapes of each tract profile were very consistent across the different age groups. Shape was preserved though mean tract values varied.

Discussion

We used a novel, automated dMRI tractography method to identify the cerebellar peduncles and to characterize age-related differences in diffusion properties across the entirety of childhood, from infancy through adolescence. In accordance with our hypothesis, mean tract-FA values increased from birth to 17 years of age while mean tract-MD values decreased. For both dMRI metrics, we observed greater changes in the first 24 months of life that rapidly stabilized beginning in the preschool period and into adolescence; this trend was described by a logarithmic function. The shape of tract profiles was stable within each cerebellar peduncle over this age range. However, the pattern of age-related differences in mean tract-FA and mean tract-MD varied among the peduncles.

Age-Related Characteristics of the Cerebellar Peduncles

Age-related changes in dMRI metrics of the cerebellar peduncles were consistent with those observed in cerebral white matter pathways, which show an increase in anisotropy paralleled by a decrease in diffusion [22, 38]. While these changes slowed down after 24 months of age, characterized by a logarithmic function, the ongoing increase in mean tract-FA and decrease in mean tract-MD indicate that the cerebellar peduncles continue to mature during late childhood and adolescence.

Few previous studies have examined cerebellar white mater across different ages [20, 23, 39], and fewer still have focused on the cerebellar peduncles [24, 25]. Saksena and colleagues [23] compared age-related changes in FA and MD obtained from cerebral and cerebellar white matter regions in children aged 0.2 to 132 months using a conventional single ROI-based approach. Similar to our findings, they showed that FA increased while MD decreased with age and that a log-linear model best described the changes in the dMRI metrics. In 3- to 60-month-old children, Deoni et al. [20] demonstrated the same trend in cerebellar white matter development using myelin water fraction imaging. In this study, we used dMRI tractography, as opposed to ROI-based analyses, and replicated the pattern of rapid change in white matter microstructure during infancy followed by a more gradual change during late childhood/adolescence. From a methodological point of view, the dMRI tractography should be preferred because (i) white matter pathways can be better delineated using a tracking approach thus reducing partial volume effects, (ii) white matter pathways can be analyzed as a whole rather than being reduced to a small region, which enables a more detailed study of white matter characteristics, and (iii) dMRI tractography demonstrates improved reproducibility over manual ROI measurements and is less subject to intra-operator variability [40]. Reproducibility is an important requirement for both comparative studies that examine white matter differences among individuals and longitudinal studies that characterize white matter development or training/therapy-related white matter changes. In addition, we created tract profiles of the middle, inferior, and superior cerebellar peduncles providing a continuous quantification of dMRI metrics along the tract. Microstructural properties may

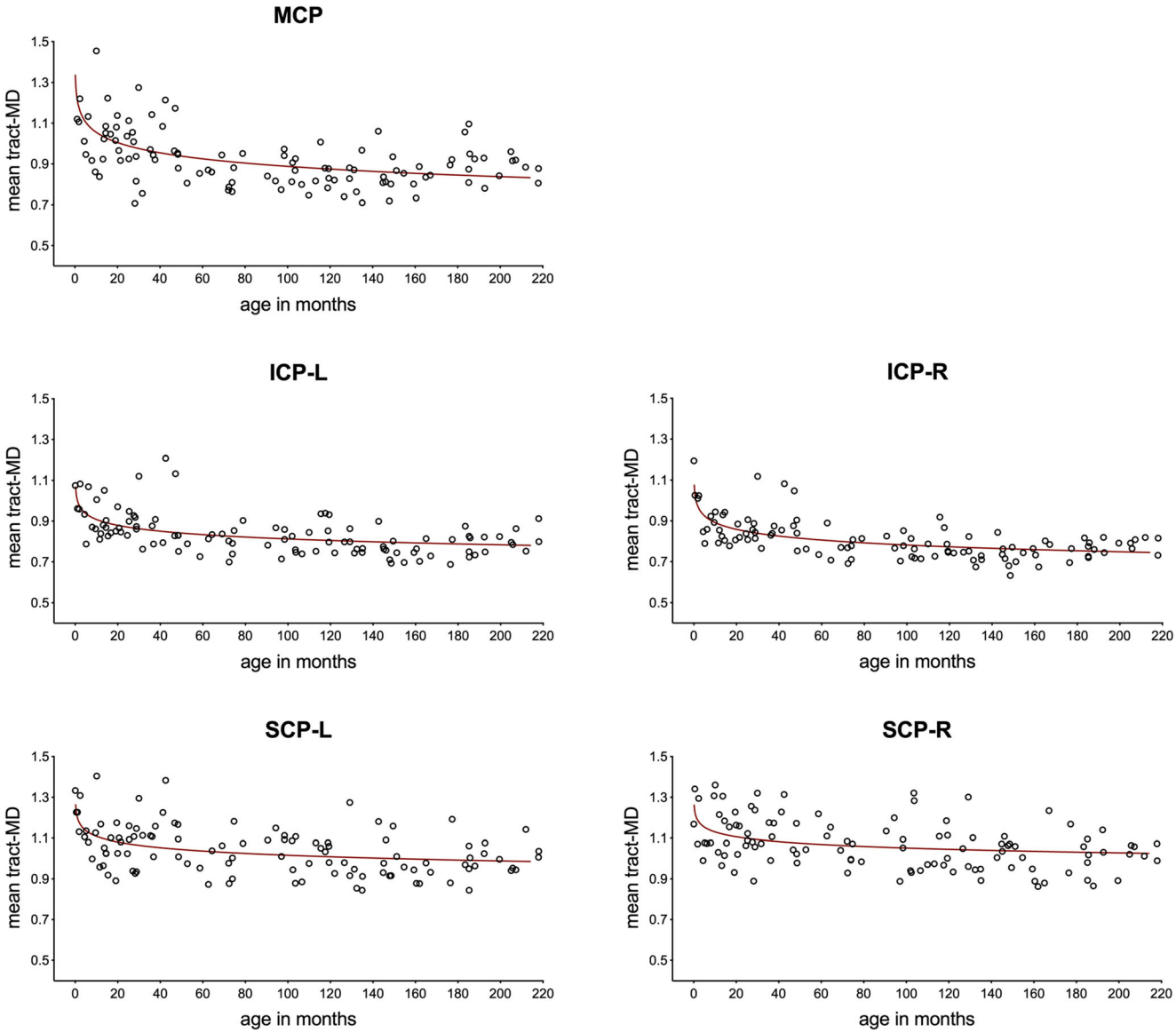

Fig. 5 Relationship between mean diffusivity (MD) and age in the cerebellar peduncles of children ranging in age from birth to 17 years (214 months). Red line shows the logarithmic curve estimation. *MCP* middle cerebellar peduncle, *ICP* inferior cerebellar peduncle, *SCP* superior cerebellar peduncle, *L* left, *R* right

not change in unison across the entire trajectory of a cerebellar pathway. Within-tract differences in FA or MD, which can be detected by comparing tract profiles but not mean tract-dMRI metrics, could reflect unique rates of white matter maturation due to local differences in supporting glia structure [41] or biochemistry throughout the brain [42].

In this study, we showed for the first time that variation in FA and MD along each cerebellar peduncle, seen at older ages, is already present in early infancy. The tract profiles were highly similar to those of two other studies that used dMRI tractography to identify the cerebellar peduncles and to assess the variability of dMRI metrics along the peduncles in a sample of 9–17-year-old children and adolescents [24, 25]. The systematic variations in dMRI metrics along the trajectory of each cerebellar peduncle are also in agreement with patterns observed in adults [15]. Like in cerebral pathways, the variation in dMRI metrics can be explained by anatomical features, such as the presence and density of crossing fibers, tract curvature, or narrowing of the tracts [26]. Age, however, was not associated with differences in cerebellar tract profiles in older children and adolescents [24, 25]. The developmental pattern described in this and in previous studies [20, 23], namely the rapid white matter change in early childhood which attenuates during adolescence, may explain the lack of age-related differences in their 9–17-year-old participants.

Table 3 Post hoc comparisons of ANOVA analyses of mean tract-FA among five age groups

	Group	*n*	*M*	SD	Significance level of Tukey HSD/Games-Howell comparisons			
					Infants	Preschoolers	Young school age	Middle school age
MCP	Infants	22	0.38	0.085				
	Preschoolers	23	0.47	0.067	**0.002**			
	Young school age	19	0.53	0.046	**< 0.0005**	**0.021**		
	Middle school age	24	0.51	0.047	**< 0.0005**	0.212	0.660	
	Adolescents	22	0.49	0.047	**< 0.0005**	0.880	0.068	0.587
ICP-L	Infants	22	0.32	0.059				
	Preschoolers	21	0.37	0.055	**0.016**			
	Young school age	18	0.41	0.064	**< 0.0005**	.131		
	Middle school age	24	0.41	0.052	**< 0.0005**	0.144	1.00	
	Adolescents	22	0.44	0.042	**< 0.0005**	**0.001**	0.476	0.279
ICP-R	Infants	20	0.32	0.069				
	Preschoolers	21	0.38	0.048	**0.009**			
	Young school age	19	0.43	0.054	**< 0.0005**	**0.012**		
	Middle school age	24	0.44	0.051	**< 0.0005**	**0.001**	0.971	
	Adolescents	22	0.42	0.050	**< 0.0005**	0.103	0.898	0.501
SCP-L	Infants	24	0.32	0.068				
	Preschoolers	22	0.38	0.060	**0.023**			
	Young school age	19	0.39	0.058	**0.006**	0.980		
	Middle school age	24	0.43	0.036	**< 0.0005**	**0.008**	0.057	
	Adolescents	22	0.44	0.035	**< 0.0005**	**0.002**	**0.019**	0.955
SCP-R	Infants	23	0.31	0.060				
	Preschoolers	22	0.37	0.036	**0.003**			
	Young school age	19	0.39	0.050	**< 0.0005**	0.428		
	Middle school age	24	0.41	0.043	**< 0.0005**	**0.024**	0.765	
	Adolescents	22	0.43	0.048	**< 0.0005**	**0.001**	0.173	0.778

n sample size, *M* mean, *SD* standard deviation, *MCP* middle cerebellar peduncle, *ICP* inferior cerebellar peduncle, *SCP* superior cerebellar peduncle, *L* left, *R* right, significant *p*-values are printed in bold

Sensitivity of FA and MD

In this study, dMRI metrics were sensitive in detecting age-related white matter differences in the cerebellar peduncles. An increase in anisotropy, as indexed by FA, combined with a decrease in diffusion, as indexed by MD, is thought to be associated with white matter maturation by means of myelination [22]. Using myelin water fraction imaging, Deoni and colleagues [20] described regional cerebral and cerebellar myelination trajectories in a large sample of healthy children aged 3 to 60 months ($n = 153$). The spatio-temporal pattern of myelination, which spread caudocranially from primary white matter tracts beginning in the cerebellum and internal capsule to superficial white matter and gray matter regions, closely resembled histological studies of brain maturation [43, 44]. In line with our findings, the progressive advancement of myelination was characterized by exponential growth over the first 12–16 months and slower growth after 2 years of age [20]. While FA and MD are highly sensitive to alterations in white matter microstructure, they are not specific. Hence, we should be careful in ascribing changes in dMRI metrics solely to changes in myelin content. Alterations in FA or MD of the cerebellar peduncles could also reflect an increase in the compactness of axonal bundles, more coherent fiber organization, or an increase in axonal diameter. The lack of specificity of FA and MD to microstructure is well known; future research should combine dMRI metrics with other neuroimaging techniques that assess myelin content [45], axonal caliber [46], or proportion of crossing fibers [47–49] to triangulate the underlying biological mechanisms.

We demonstrated that the increase and decrease in both dMRI metrics followed a logarithmic shape. However, the model explained more of the variance in FA compared to MD measures. Discrepancies between FA and MD trajectories may reflect differences in the sensitivity of these dMRI metrics to underlying physiologic processes. Increases in FA are thought to be related to increased white matter integrity of a tract, whereas decreases in MD may be more sensitive to

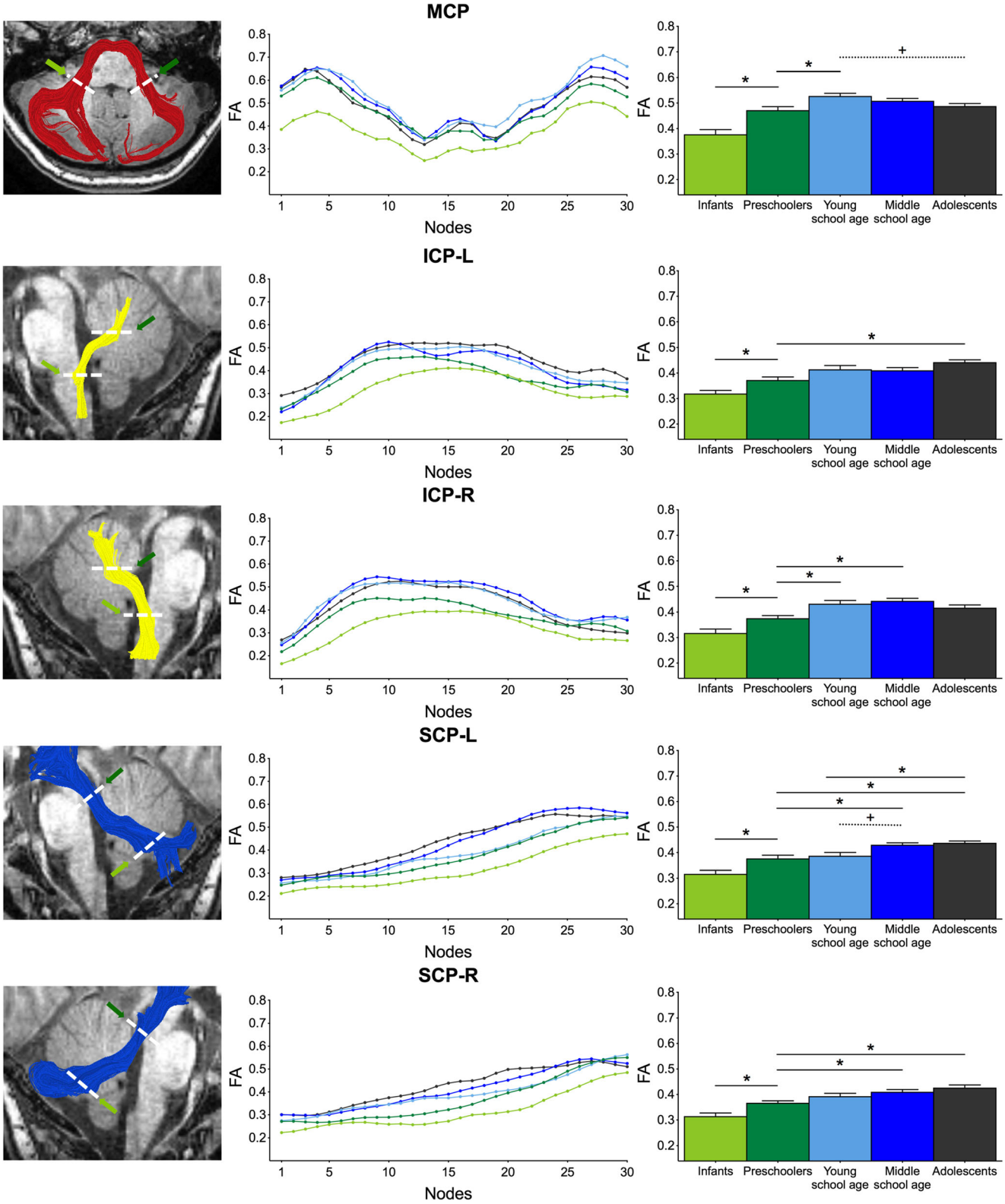
MCP
ICP-L
ICP-R
SCP-L
SCP-R
FA
Nodes
Infants
Preschoolers
Young school age
Middle school age
Adolescents

Table 4 Post hoc comparisons of ANOVA analyses of mean tract-MD among five age groups

	Group	*n*	*M*	SD	Significance level of Tukey HSD/Games-Howell comparisons			
					Infants	Preschoolers	Young school age	Middle school age
MCP	Infants	22	1.07	0.176				
	Preschoolers	23	0.98	0.145	0.277			
	Young school age	19	0.86	0.068	**< 0.0005**	**0.011**		
	Middle school age	24	0.84	0.087	**< 0.0005**	**0.004**	0.965	
	Adolescents	22	0.89	0.085	**0.001**	0.106	0.701	0.375
ICP-L	Infants	22	0.92	0.092				
	Preschoolers	21	0.89	0.128	0.894			
	Young school age	18	0.80	0.057	**< 0.0005**	0.062		
	Middle school age	24	0.80	0.074	**< 0.0005**	0.060	1.00	
	Adolescents	22	0.79	0.057	**< 0.0005**	**0.021**	0.950	0.979
ICP-R	Infants	20	0.90	0.105				
	Preschoolers	21	0.87	0.102	0.898			
	Young school age	19	0.77	0.056	**< 0.0005**	**0.004**		
	Middle school age	24	0.75	0.063	**< 0.0005**	**0.001**	0.903	
	Adolescents	22	0.77	0.041	**< 0.0005**	**0.002**	1.00	0.856
SCP-L	Infants	24	1.11	0.129				
	Preschoolers	22	1.10	0.119	0.997			
	Young school age	19	1.02	0.100	0.070	0.163		
	Middle school age	24	1.00	0.105	**0.010**	**0.035**	0.988	
	Adolescents	22	0.98	0.085	**0.002**	**0.007**	0.819	0.969
SCP-R	Infants	23	1.14	0.125				
	Preschoolers	22	1.12	0.112	0.979			
	Young school age	19	1.06	0.121	0.153	0.417		
	Middle school age	24	1.03	0.091	**0.013**	0.072	0.941	
	Adolescents	22	1.00	0.103	**0.001**	**0.007**	0.497	0.891

n sample size, *M* mean, *SD* standard deviation, *MCP* middle cerebellar peduncle, *ICP* inferior cerebellar peduncle, *SCP* superior cerebellar peduncle, *L* left, *R* right, significant p-values are printed in bold

decreased volume of extracellular space or total brain water content [50–53].

◀ **Fig. 6** FA tract profiles of the cerebellar peduncles. Left hand column shows renderings of each cerebellar peduncle on an axial (MCP) or sagittal (ICP, SCP) T1-weighted images of the same representative subject shown in Fig. 3. Middle column shows FA tract profiles for infants (light green), preschoolers (dark green), young school-aged children (light blue), middle school-aged children (dark blue), and adolescents (dark gray). FA values are plotted for 30 equidistant locations between two defining ROIs as indicated by dashed white lines. Right hand column shows mean tract-FA of the cerebellar peduncles plotted for each age group. Error bars indicate the standard error of the mean (SEM). Significant differences in mean tract-FA among the five age groups as assessed by post hoc comparisons are indicated by an asterisk ($p < 0.05$). *MCP* middle cerebellar peduncle, *ICP* inferior cerebellar peduncle, *SCP* superior cerebellar peduncle, *L* left, *R* right

Limitations and Future Directions

One limitation of the study is that the sample size was modest and thus might not be adequate to describe the true variation in dMRI metrics across and especially within different age groups. However, our sample size is comparable to other neuroimaging studies of development and our finding that FA increase and MD decrease follow a logarithmic trend is in good agreement with other studies of brain maturation [20, 23, 39]. To validate this normative data, future studies should investigate whether the pattern of age-related change observed in the cerebellar peduncles persists in larger samples. Because the dMRI protocol is part of the standard clinical care at our institution, we are able to add new scans over time.

Another limitation relates to the use of cross-sectional rather than longitudinal data to evaluate age-related change in dMRI metrics. Because cross-sectional data does not take

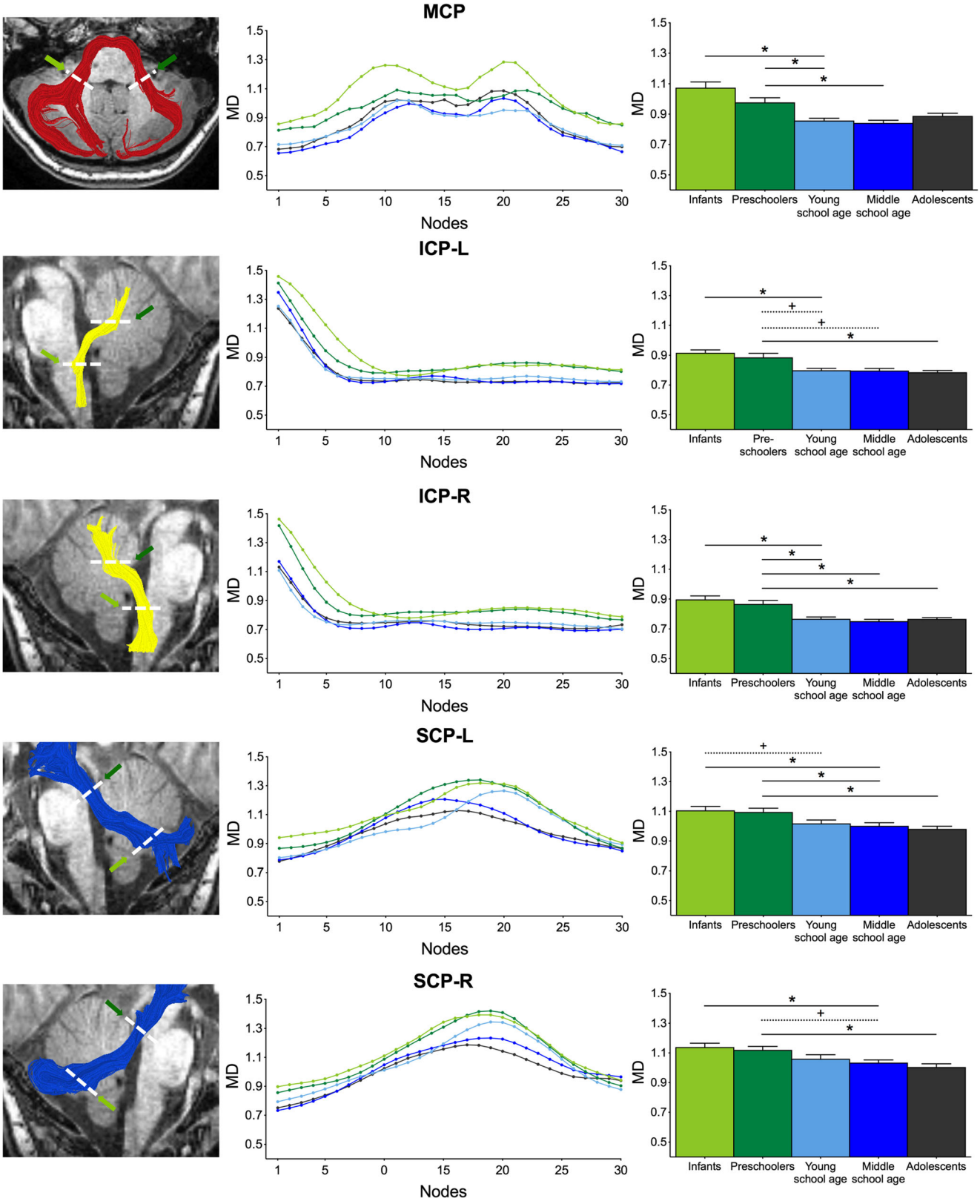
MCP
ICP-L
ICP-R
SCP-L
SCP-R
MD
Nodes
Infants
Preschoolers
Pre-schoolers
Young school age
Middle school age
Adolescents

◀ **Fig. 7** MD tract profiles of the cerebellar peduncles. Left hand column shows renderings of each cerebellar peduncle on an axial (MCP) or sagittal (ICP, SCP) T1-weighted images of the same representative subject shown in Fig. 3. Middle column shows MD tract profiles for infants (light green), preschoolers (dark green), young school-aged children (light blue), middle school-aged children (dark blue), and adolescents (dark gray). MD values are plotted for 30 equidistant locations between two defining ROIs as indicated by dashed white lines. Right hand column shows mean tract-MD of the cerebellar peduncles plotted for each age group. Error bars indicate the standard error of the mean (SEM). Significant differences in mean tract-MD among the five age groups as assessed by post hoc comparisons are indicated by an asterisk ($p < 0.05$). *MCP* middle cerebellar peduncle, *ICP* inferior cerebellar peduncle, *SCP* superior cerebellar peduncle, *L* left, *R* right

interindividual differences into account, our results do not permit us to draw longitudinal inferences about the developmental trajectory of the cerebellar peduncles. In this study, we capitalized on the availability of scans acquired in children being screened for any brain abnormality. This factor may in and of itself make the scans unrepresentative of a community-based sample. However, our strict inclusion and exclusion criteria make this possibility unlikely. Since scans and follow-up reports of all our participants were normal, no additional scans were obtained. Applying our methods to longitudinal data would provide detailed information about intraindividual change and interindividual differences in intraindividual change, which could be used to establish normative growth curves of the cerebellar peduncles. In addition, longitudinal analysis of children from clinical populations is necessary to determine if these methods assist in identifying specific abnormalities in children with conditions affecting the cerebellum or cerebellar pathways, such as children with posterior fossa tumors. Comparing clinical populations to typically developing children in future studies will allow us to evaluate the clinical utility of our findings.

Both mean tract-dMRI metrics and tract profiles may provide a comprehensive set of age-related white matter characteristics against which an individual or a clinical population can be measured. Although it is difficult to compare absolute FA or MD values across different scanners and dMRI protocols, the *z* scores of a single patient in relation to a normative sample from the same scanner may be comparable across sites. Future studies should include strategies for normalizing dMRI metrics (e.g., through the use of phantoms [54, 55]) in order to develop normative data that can be used by clinicians and researchers across different scanners.

Conclusion

The development of cerebellum-cerebrum connections is essential for motor and cognitive functions. In this study, we have outlined new automated dMRI tractography methods that were designed to successfully identify and characterize the middle, inferior, and superior cerebellar peduncles in infancy, childhood, and adolescence. We think that these methods may prove useful for other studies of the cerebellar circuitry and will be made publicly available at https://github.com/yeatmanlab/AFQ/tree/master/cerebellarPeduncles. For the first time, we have described age-related differences in microstructural properties of the cerebellar peduncles across the spectrum of development using dMRI tractography. Mean diffusion properties and variations along each of the peduncles provide a rich normative data set of cerebellar white matter characteristics across different ages from infancy to adolescence. This information will be helpful for assessing and understanding variations in the cerebellar circuitry in clinical populations. Comparing cerebellar white matter characteristics of pediatric patients to typically developing children may lead to identification of sensitive biomarkers of specific developmental conditions.

Funding This study was funded by the following grants: Eunice Kennedy Shriver National Institute of Child Health and Human Development of the National Institutes of Health (RO1 HD069162 to Feldman, PI and 5K99HD084749 to Travis, PI) and the Stanford Transdisciplinary Initiatives Program, Child Health Research Institute (1186741-100-DHDHY).

Compliance with Ethical Standards

Conflict of Interest The authors declare that they have no conflict of interest.

References

1. Manto M, Bower JM, Conforto AB, Delgado-García JM, da Guarda SNF, Gerwig M, et al. Consensus paper: roles of the cerebellum in motor control—the diversity of ideas on cerebellar involvement in movement. Cerebellum. 2012;11(2):457–87.
2. Schmahmann JD. The role of the cerebellum in cognition and emotion: personal reflections since 1982 on the dysmetria of thought hypothesis, and its historical evolution from theory to therapy. Neuropsychol Rev. 2010;20(3):236–60.
3. Stoodley CJ. The cerebellum and cognition: evidence from functional imaging studies. Cerebellum. 2012;11(2):352–65.
4. Strick PL, Dum RP, Fiez JA. Cerebellum and nonmotor function. Annu Rev Neurosci. 2009;32:413–34.
5. Levisohn L, Cronin-Golomb A, Schmahmann JD. Neuropsychological consequences of cerebellar tumour resection in children. Brain. 2000;123(5):1041–50.
6. Schmahmann JD. Disorders of the cerebellum: ataxia, dysmetria of thought, and the cerebellar cognitive affective syndrome. J Neuropsychiatry Clin Neurosci. 2004;16(3):367–78.
7. Schmahmann JD, Sherman JC. The cerebellar cognitive affective syndrome. Brain. 1998;121(4):561–79.
8. Tavano A, Grasso R, Gagliardi C, Triulzi F, Bresolin N, Fabbro F, et al. Disorders of cognitive and affective development in cerebellar malformations. Brain. 2007;130(10):2646–60.

9. Arora RS, Alston RD, Eden TOB, Estlin EJ, Moran A, Birch JM. Age–incidence patterns of primary CNS tumors in children, adolescents. and adults in England Neuro Oncol. 2009;11(4):403–13.
10. Limperopoulos C, Soul JS, Gauvreau K, Huppi PS, Warfield SK, Bassan H, et al. Late gestation cerebellar growth is rapid and impeded by premature birth. Pediatrics. 2005;115(3):688–95.
11. Messerschmidt A, Prayer D, Brugger PC, Boltshauser E, Zoder G, Sterniste W, et al. Preterm birth and disruptive cerebellar development: assessment of perinatal risk factors. Eur J Paediatr Neurol. 2008;12(6):455–60.
12. Volpe JJ. Brain injury in premature infants: a complex amalgam of destructive and developmental disturbances. Lancet Neurol. 2009;8(1):110–24.
13. Fatemi SH, Aldinger KA, Ashwood P, Bauman ML, Blaha CD, Blatt GJ, et al. Consensus paper: pathological role of the cerebellum in autism. Cerebellum. 2012;11(3):777–807.
14. Naidich TP, Duvernoy HM. Duvernoy's atlas of the human brain stem and cerebellum: high-field MRI : surface anatomy, internal structure, vascularization and 3D sectional anatomy. Springer; 2009. 876 p.
15. Stieltjes B, Kaufmann WE, van Zijl PCM, Fredericksen K, Pearlson GD, Solaiyappan M, et al. Diffusion tensor imaging and axonal tracking in the human brainstem. Neuroimage. 2001;14(3):723–35.
16. Messerschmidt A, Brugger PC, Boltshauser E, Zoder G, Sterniste W, Birnbacher R, et al. Disruption of cerebellar development: potential complication of extreme prematurity. Am J Neuroradiol. 2005;26(7):1659–67.
17. Nopoulos PC, Conrad AL, Bell EF, Strauss RG, Widness JA, Magnotta VA, et al. Long-term outcome of brain structure in premature infants. Arch Pediatr Adolesc Med. 2011;165(5):443–50.
18. Limperopoulos C. Impaired trophic interactions between the cerebellum and the cerebrum among preterm infants. Pediatrics. 2005;116(4):844–50.
19. Diedrichsen J, Balsters JH, Flavell J, Cussans E, Ramnani N. A probabilistic MR atlas of the human cerebellum. Neuroimage. 2009;46(1):39–46.
20. Deoni SCL, Dean DC, O'Muircheartaigh J, Dirks H, Jerskey BA. Investigating white matter development in infancy and early childhood using myelin water faction and relaxation time mapping. Neuroimage. 2012;63(3):1038–53.
21. Barnea-Goraly N, Menon V, Eckert M, Tamm L, Bammer R, Karchemskiy A, et al. White matter development during childhood and adolescence: a cross-sectional diffusion tensor imaging study. Cereb Cortex. 2005 Dec;15(12):1848–54.
22. Mukherjee P, Miller JH, Shimony JS, Conturo TE, Lee BC, Almli CR, et al. Normal brain maturation during childhood: developmental trends characterized with diffusion-tensor MR imaging. Radiology. 2001;221(2):349–58.
23. Saksena S, Husain N, Malik GK, Trivedi R, Sarma M, Rathore RS, et al. Comparative evaluation of the cerebral and cerebellar white matter development in pediatric age group using quantitative diffusion tensor imaging. Cerebellum. 2008;7(3):392–400.
24. Leitner Y, Travis KE, Ben-Shachar M, Yeom KW, Feldman HM. Tract profiles of the cerebellar white matter pathways in children and adolescents. Cerebellum. 2015;14(6):613–23.
25. Travis KE, Leitner Y, Feldman HM, Ben-Shachar M. Cerebellar white matter pathways are associated with reading skills in children and adolescents. Hum Brain Mapp. 2015;36(4):1536–53.
26. Yeatman JD, Dougherty RF, Myall NJ, Wandell BA, Feldman HM. Tract profiles of white matter properties: automating fiber-tract quantification. PLoS One. 2012;7(11).
27. Just MA, Keller TA, Malave VL, Kana RK, Varma S. Autism as a neural systems disorder: a theory of frontal-posterior underconnectivity. Neurosci Biobehav Rev. 2012;36(4):1292–313.
28. Meda SA, Gill A, Stevens MC, Lorenzoni RP, Glahn DC, Calhoun VD, et al. Differences in resting-state functional magnetic resonance imaging functional network connectivity between schizophrenia and psychotic bipolar probands and their unaffected first-degree relatives. Biol Psychiatry. 2012;71(10):881–9.
29. Rohde GK, Barnett AS, Basser PJ, Marenco S, Pierpaoli C. Comprehensive approach for correction of motion and distortion in diffusion-weighted MRI. Magn Reson Med. 2004;51(1):103–14.
30. Oouchi H, Yamada K, Sakai K, Kizu O, Kubota T, Ito H, et al. Diffusion anisotropy measurement of brain white matter is affected by voxel size: underestimation occurs in areas with crossing fibers. Am J Neuroradiol. 2007;28(6):1102–6.
31. Leemans A, Jones DK. The B-matrix must be rotated when correcting for subject motion in DTI data. Magn Reson Med. 2009;61(6):1336–49.
32. Mori S, Crain BJ, Chacko VP, van Zijl PC. Three-dimensional tracking of axonal projections in the brain by magnetic resonance imaging. Ann Neurol. 1999;45(2):265–9.
33. Rose J, Vassar R, Cahill-Rowley K, Guzman XS, Stevenson DK, Barnea-Goraly N. Brain microstructural development at near-term age in very-low-birth-weight preterm infants: an atlas-based diffusion imaging study. Neuroimage. 2014;86:244–56.
34. de Bruïne FT, van Wezel-Meijler G, Leijser LM, van den Berg-Huysmans AA, van Steenis A, van Buchem MA, et al. Tractography of developing white matter of the internal capsule and corpus callusom in very preterm infants. Eur Radiol. 2011;21(3):538–47.
35. Friston KJ, Ashburner J. Generative and recognition models for neuroanatomy. Neuroimage. 2004;23(1):21–4.
36. Dodson CK, Travis KE, Ben-Shachar M, Feldman HM. White matter microstructure of 6-year old children born preterm and full term. NeuroImage Clin. 2017;16:268–75.
37. Fingher N, Dinstein I, Ben-Shachar M, Haar S, Dale AM, Eyler L, et al. Toddlers later diagnosed with autism exhibit multiple structural abnormalities in temporal corpus callosum fibers. Cortex. 2017;97:291–305.
38. Schneider JFL, Il'yasov KA, Hennig J, Martin E. Fast quantitative diffusion-tensor imaging of cerebral white matter from the neonatal period to adolescence. Neuroradiology. 2004;46(4):258–66.
39. Dubois J, Hertz-Pannier L, Dehaene-Lambertz G, Cointepas Y, Le Bihan D. Assessment of the early organization and maturation of infants' cerebral white matter fiber bundles: a feasibility study using quantitative diffusion tensor imaging and tractography. Neuroimage. 2006;30(4):1121–32.
40. Partridge SC, Mukherjee P, Berman JI, Henry RG, Miller SP, Lu Y, et al. Tractography-based quantitation of diffusion tensor imaging parameters in white matter tracts of preterm newborns. J Magn Reson Imaging. 2005;22(4):467–74.
41. Yeh T-H, Lee DY, Gianino SM, Gutmann DH. Microarray analyses reveal regional astrocyte heterogeneity with implications for neurofibromatosis type 1 (NF1)-regulated glial proliferation. Glia. 2009;57(11):1239–49.
42. Vasung L, Huang H, Jovanov-Milošević N, Pletikos M, Mori S, Kostović I. Development of axonal pathways in the human fetal fronto-limbic brain: histochemical characterization and diffusion tensor imaging. J Anat. 2010;217(4):400–17.
43. Yakovlev P, Lecours A. The myelogenetic cycles of regional maturation of the brain. Regional development of the brain in early life. 1967.
44. Kinney HC, Brody BA, Kloman AS, Gilles FH. Sequence of central nervous system myelination in human infancy. II. Patterns of myelination in autopsied infants. J Neuropathol Exp Neurol. 1988;47(3):217–34.
45. Mezer A, Yeatman JD, Stikov N, Kay KN, Cho N, Dougherty RF, et al. Quantifying the local tissue volume and composition in individual brains with MRI HHS Public Access. Nat Med. 2013;19(12):1667–72.

46. Assaf Y, Blumenfeld-Katzir T, Yovel Y, Basser PJ. Axcaliber: a method for measuring axon diameter distribution from diffusion MRI. Magn Reson Med. 2008;59(6):1347–54.
47. Tournier J-D, Yeh C-H, Calamante F, Cho K-H, Connelly A, Lin C-P. Resolving crossing fibres using constrained spherical deconvolution: validation using diffusion-weighted imaging phantom data. Neuroimage. 2008;42(2):617–25.
48. Tuch DS, Reese TG, Wiegell MR, Makris N, Belliveau JW, Wedeen VJ. High angular resolution diffusion imaging reveals intravoxel white matter fiber heterogeneity. Magn Reson Med. 2002;48(4):577–82.
49. Zhang H, Schneider T, Wheeler-Kingshott CA, Alexander DC. NODDI: practical in vivo neurite orientation dispersion and density imaging of the human brain. Neuroimage. 2012;61(4):1000–16.
50. Beaulieu C. The basis of anisotropic water diffusion in the nervous system—a technical review. NMR Biomed. 2002;15(7–8):435–55.
51. Morriss MC, Zimmerman RA, Bilaniuk LT, Hunter JV, Haselgrove JC. Changes in brain water diffusion during childhood. Neuroradiology. 1999;41(12):929–34.
52. Giorgio A, Watkins KE, Chadwick M, James S, Winmill L, Douaud G, et al. Longitudinal changes in grey and white matter during adolescence. NeuroImage. 2010;49(1):94–103.
53. Hermoye L, Saint-Martin C, Cosnard G, Lee S-K, Kim J, Nassogne M-C, et al. Pediatric diffusion tensor imaging: normal database and observation of the white matter maturation in early childhood. Neuroimage. 2006;29(2):493–504.
54. Doshi J, Erus G, Ou Y, Resnick SM, Gur RC, Gur RE, et al. MUSE: MUlti-atlas region Segmentation utilizing Ensembles of registration algorithms and parameters, and locally optimal atlas selection. Neuroimage. 2016;127:186–95.
55. Iglesias JE, Sabuncu MR. Multi-atlas segmentation of biomedical images: a survey. Med Image Anal. 2015;24(1):205–19.